

Photophysics of a *Cis* Axially Disubstituted Macrocycle: Rapid Intersystem Crossing in a Sn^{IV} Phthalocyanine with a Half-Domed Geometry

Elizabeth Gutiérrez-Meza,[†] Raquel Noria,[†] Gilma Granados,[†] Virginia Gómez-Vidales,[†] José Zeferino Ramírez,[‡] Hirám Isaac Beltrán,[§] and Jorge Peon^{*,†}

[†]Universidad Nacional Autónoma de México, Instituto de Química, Ciudad Universitaria, 04510, México, D.F., México

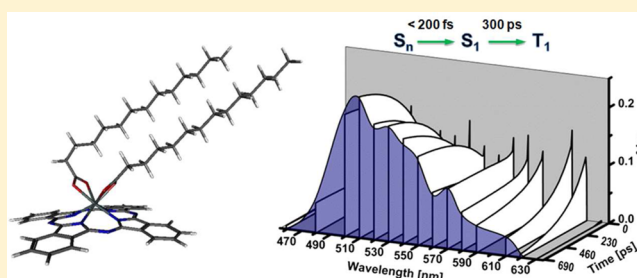
[‡]Universidad de Sonora, Unidad Regional Centro, Col. Centro, C.P. 83000, Hermosillo, Sonora, México

[§]Departamento de Ciencias Naturales, DCNI, Universidad Autónoma Metropolitana, Unidad Cuajimalpa, Av. Pedro Antonio de los Santos 84, 11850 México D. F., México

S Supporting Information

ABSTRACT: We have studied the photophysical properties of a tin^{IV} phthalocyanine which coordinates two myristate groups through their carboxylate functionalities in a *cis* disposition at the tin center. Such a coordination mode, anisobidentate through the same side of the macrocycle, makes this phthalocyanine acquire a capped or half-domed shape. This *bis* myristate tin^{IV} molecule shows an intersystem crossing channel which populates the triplet manifold with high efficiency and with a time constant of 300 ps, about an order of magnitude faster than planar phthalocyanines, including some previously reported tin^{IV} phthalocyanines.

For comparison purposes, we also include the description of a planar $\text{silicon}^{\text{IV}}$ phthalocyanine that keeps the more common stereochemistry, of *trans* type, with the same axial myristate groups. The characterization of these systems included steady state and time-resolved spectroscopy through femtosecond fluorescence up-conversion and transient absorption. We also studied the initial $S_n \rightarrow S_1$ internal conversion dynamics when these compounds are excited to upper states with 387.5 nm light. In addition, we include measurements of the rate for singlet oxygen production through the formation of an ESR-active adduct in aerated solutions. Such measurements indicate that, associated to its photophysics, the tin^{IV} phthalocyanine produces $^1\text{O}_2$ with an efficiency significantly larger than the $\text{silicon}^{\text{IV}}$ counterpart, making it an interesting option for sensitization applications. Finally, we performed excited state calculations at the TD-DFT level which describe the effects of the reduced symmetry together with the state ordering and indicate the presence of near dark intermediate states between the Q and B transitions for both of these macrocycles.



INTRODUCTION

Since their discovery, phthalocyanines have had multiple applications in various fields, including as sensitizers in solar cells, chemical sensors, semiconductor devices, nonlinear optics materials, and photodynamic therapy (PDT) agents.^{1–3} This is due to their extended π electron system and related stability but especially to their unique optical and spectroscopic properties. Nevertheless, these systems often form aggregates due to strong intermolecular π – π stacking, also causing low solubility in almost any solvent, polar or non-polar. In an effort to overcome this drawback, phthalocyanines with added long hydrocarbon tails in the form of axial ligands bonded directly to the central metal core have been synthesized.^{4–7} In the present work, we studied the photophysical properties of tin^{IV} and $\text{silicon}^{\text{IV}}$ phthalocyanines both containing axial myristate chain substituents, respectively *cis*-PcSn(Myristate)₂ and *trans*-PcSi(Myristate)₂ (see Scheme 1), using steady state and temporally resolved methods. The objective herein was to understand how the

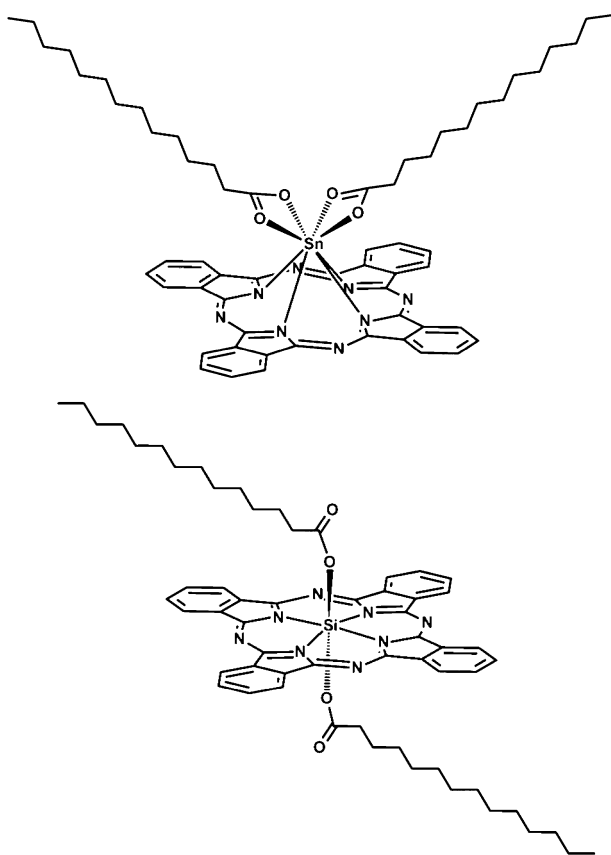
different centers and molecular geometries generated from the different kinds of axial disubstitutions may affect the pathways of decay of the singlet excited states. Principally, the photophysical properties of the tin^{IV} macrocycle are of interest, since its molecular geometry loses the typical fully planar conformation.

The size, charge, and ligand substitution of the metal center and its location with respect to the main plane of the macrocyclic system are all variables that determine the final conformation of phthalocyanines. The tin^{IV} phthalocyanine with myristate chain substituents of this study shows an interesting arrangement: the presence of the $\text{Sn}(\text{COOR})_2$ moiety induces a deformation of the phthalocyaninic macrocycle concomitant with the elongation of the N–Sn bonds,⁵

Received: August 7, 2012

Revised: October 26, 2012

Published: October 29, 2012

Scheme 1. Molecular Structures of the Compounds of This Study^a

^aTop: *cis*-PcSn(Myristate)₂. Bottom: *trans*-PcSi(Myristate)₂.

which makes the coordination number to increase from six to eight and allowing for a *cis* stereochemical disposition of the two myristate substituents. The first elucidated compound with an octa-coordinated tin atom was a tin^{IV} *bis*-phthalocyanine, where not one but two phthalocyanine ring systems formed a sandwich-type structure with the tin atom in the center.⁸ In fact, the determination of several X-ray structures of *cis*-phthalocyanine-tin^{IV} dicarboxylates has revealed octa-coordinated tin atoms with a square-antiprismatic geometry linked to the asymmetrically anisobidentate bonded COOSn moieties.⁴ As will be shown below, this bonding mode to a tin center in *cis*-PcSn(Myristate)₂ appears to have implications on the evolution of the first singlet excited state, allowing for rapid and efficient intersystem crossing (ISC), even in comparison with previously reported planar tin^{IV} macrocycles,^{9,10} and several well-known tin^{IV} compounds directly bonded to planar chromophores, many of which show long fluorescent state lifetimes.¹¹

For the silicon^{IV} phthalocyanine of Scheme 1, the central atom has a coordination number of six with two covalent and two dative resonant bonds from four nitrogen atoms and two covalent bonds with two oxygen atoms. At this molecular geometry, the silicon central atom lies at the center of an axially distorted octahedron.⁷ In this structure, the carboxylate fragments are bonded to the central atom through a covalent oxygen–silicon bond in a *trans* configuration.

Despite the detailed structural description that has been reported for both of these phthalocyanines, their photophysical properties had not been investigated, especially several aspects of their excited state dynamics. Our present study includes

femtosecond fluorescence up-conversion measurements of the internal conversion (IC, $S_n \rightarrow S_1$) upon excitation in the Soret band system with light of 387.5 nm, fluorescence state lifetime measurements (S_1), and the excited state evolution as determined by transient absorption with femtosecond resolution for *cis*-PcSn(Myristate)₂. Given the potential applications of this kind of molecules and motivated by the observed S_1 decay pathway, we have in addition measured the yields for singlet oxygen (1O_2) production after photoexcitation in a nonaqueous solvent. Our observations of the excited state processes were complemented by theoretical calculations at the DFT and TD-DFT levels of theory, which describe the excited state ordering and their character in the visible and UV regions. To our knowledge, this is the first time-resolved description of the photophysics of a dome-shaped phthalocyanine with this type of arrangement for the ligands; therefore, it was illustrative to have calculations about the kind of electronic transitions present and to compare them with the typical planar case (here, the planar *trans*-PcSi(Myristate)₂). Of particular interest are the theoretical results about the loss of degeneracy in the Q-band transitions, the verification of the presence of $n-\pi^*$ states between the spectral region of the Q-bands and the B-bands (see Results), and the overall question of whether the essential Goutermann type of description can be maintained in a deformed macrocycle with a large out-of-plane central atom like *cis*-PcSn(Myristate)₂, for the Q-band.

EXPERIMENTAL SECTION

Synthesis of *cis*-PcSn(Myristate)₂ and *trans*-PcSi(Myristate)₂. The molecules of our study were synthesized through the reaction between the chlorinated core of both phthalocyanines: *trans*-PcSnCl₂, *trans*-PcSiCl₂ and the sodium salt of myristic acid in a 1:2 molar ratio,^{6,7} and the resulting reaction mixture was refluxed in toluene for 4.5 h. The desired products were separated by filtration, evaporation of the solvent, and repeated crystallization from dichloromethane/acetonitrile mixtures to give characteristic blue powders, which were identified by the previously reported characterization (¹H NMR, UV–vis, IR).^{4,5,7}

Optical Spectroscopy. The steady state absorption and emission spectra of both phthalocyanines were taken in HPLC quality dichloromethane (Aldrich) in 1 cm quartz cells. The absorption spectra were measured with a Cary-50 spectrophotometer, and the corresponding emission spectra were measured with a Cary Eclipse spectrophotometer (Varian). Since the absorption spectrometer has a limited resolution, the details of the shape of the first absorption transition in our systems were studied through the respective excitation spectra using the emission instrument. Fluorescence quantum yields were obtained in dichloromethane using recrystallized rhodamine B (Aldrich) in methanol as a standard in solutions with an optical absorbance of less than 0.05 at the absorbance maxima. Time resolved emission experiments were carried out using the fluorescence up-conversion setup described in more detail elsewhere.³ The laser source is based on a Ti:sapphire oscillator pumped by a continuous wave laser (Verdi V5, Coherent) with a power of 5 W, to generate a 100 MHz femtosecond pulse train which was passed through an expander before its amplification. We used a regenerative amplifier operating at a 1 kHz repetition rate with 0.5 mJ pulses, which finally passed through a compressor in order to reconstruct their temporal properties. The pulses obtained centered at 775 nm, served as a gate pulse. Excitation pulses were obtained by

frequency doubling in a BBO crystal, generating the second harmonic at 387.5 nm, allowing for excitation at the edge of the B-band. The fluorescence from the sample was collected with a pair of parabolic mirrors to be optically summed with the temporally delayed 775 nm gate pulse. The sum frequency of the signal was generated in another BBO crystal; this up-conversion signal was detected through a double monochromator and photomultiplier tube and processed as indicated previously.¹² Our transient absorption setup has also been described in detail previously.¹³ We used the second harmonic of the amplified laser system for excitation in the red edge of the Soret band system, and generated a continuum in a 1 mm sapphire disk to form probe light. Pump–probe experiments were performed with magic angle conditions detecting the different wavelengths of the continuum with the aid of a monochromator and an amplified silicon photodiode. The pump beam was modulated at 1/3 of the laser repetition rate with a phase adjustable chopper in order to monitor the intensity modulations with a lock-in amplifier as described in previous references.^{14,15}

Singlet Oxygen Yields. The measurements for the production of singlet oxygen by ESR were carried out at room temperature with a Jeol JES-TE300 spectrophotometer system operating at X band, 100 kHz modulation frequency and a cylindrical cavity in the mode TE₀₁₁. The external calibration of the magnetic field was made with a precision gaussmeter, Jeol ES-FC5. The spectrometer settings for all spectra were as follows: center field, 336.2 mT; microwave frequency, 9.43 GHz; sweep width, ± 4 mT; modulation width, 0.79×0.1 mT; time constant, 0.1 s; amplitude, 200. Spectral acquisition and manipulations were performed using the program ES-IPRITS/TE.

The experiments to measure the photogeneration of $^1\text{O}_2$ were carried out in a flat cell (synthetic quartz, Willmad Glass Company) of 0.2 mm by 5 mm. A 1000 W Hg lamp (ES-USH10) and a Schott interference filter, type RG 610, which transmitted light over the 590–800 nm range was used. The incident photon flux was determined by chemical actinometry using potassium reineckate in the exact same disposition in the ESR instrument.¹⁶ The detection of $^1\text{O}_2$ was carried out by adding an amount of *cis*-PcSn(My_r)₂ or *trans*-PcSi(My_r)₂ sensitizer (0.03–0.06 mM) to a 30 mM 2,2,6,6-tetramethyl-1-piperidine (TEMP) solution in air-equilibrated ethanol. Samples were placed in the quartz ESR cell, and positioned in the sample holder. In each case, the ESR parameters were held constant, as was the concentration of TEMP. Samples were irradiated with red light ($590 \text{ nm} < \lambda < 800 \text{ nm}$) for up to 30 min (power at the sample $< 0.1 \text{ mW}$) directly within the ESR cavity. By comparison of the ESR integrated intensity with that of the known concentration of commercial 2,2,6,6-tetramethylpiperidine-1-oxyl (TEMPO, Aldrich), the amount of produced TEMPO from photochemical reaction was determined.

Computational Section. The structures of *trans*-PcSi(My_r)₂ and *cis*-PcSn(My_r)₂ were initially taken from their reported crystallographic structures,^{4,5,7} and were fully optimized to equilibrium geometries using the PBE functional^{17,18} and the 3-21G basis set.^{19–22} Although this basis set is small, it produces very similar geometries in comparison with the diffraction data (see Results). In addition, it has been established recently that small changes in the geometries of phthalocyanines have only minor effects in the transition energies and the state and orbital orderings.²³ The optimization

was followed by a TD-DFT single-point calculation at the PBE/6-311++G level for each structure,^{24,25} including CRENBL ECP for Sn.^{26,27} The NWChem 5.1.1 program suite was applied to perform all theoretical calculations.^{28,29} The choice of the PBE functional is substantiated in recent TD-DFT calculations which indicate that both pure and hybrid exchange-correlation functionals produce good agreement with the observed spectra, giving consistent descriptions in terms of transition energies and the orbitals involved in the different transitions.²³

RESULTS AND DISCUSSION

Steady State Spectroscopy. Absorption and fluorescence spectra of dichloromethane solutions of *cis*-PcSn(My_r)₂ and the *trans*-PcSi(My_r)₂ phthalocyanines are shown in Figure 1. In the

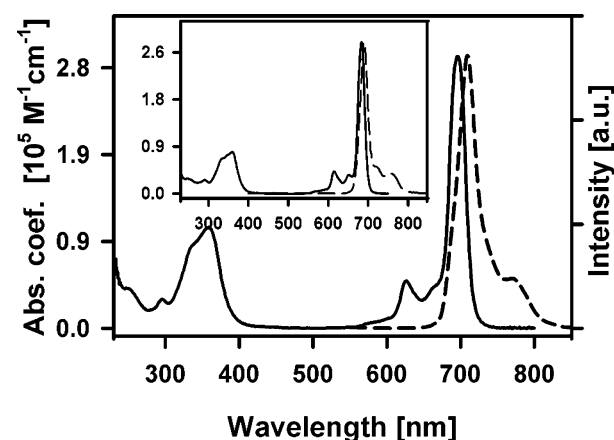


Figure 1. Absorption (solid lines) and fluorescence emission (dashed lines) spectra of the phthalocyanines of this study: *cis*-PcSn(My_r)₂ (main plot) and *trans*-PcSi(My_r)₂ (inset).

absorption spectra, the $S_1 \leftarrow S_0$ and $S_n \leftarrow S_0$ transitions corresponding to the Q and Soret bands at 680–720 and 300–400 nm, respectively, are typical of this kind of macrocycles, which indicates that despite the half-domed geometry obtained with *cis* disposition of the ligands in *cis*-PcSn(My_r)₂, and respective symmetry alterations, the important light absorption properties are maintained. For the emission spectra, the $S_1 \rightarrow S_0$ transition steady state emission is centered at 680–700 nm, and maintains the common vibroelectronic band shapes for both phthalocyanines. Fluorescence excitation spectra are shown in Figure 2, where each spectrum is presented together with the fluorescence excitation spectra of zinc phthalocyanine (PcZn), allowing for comparisons with a highly symmetric D_{4h} phthalocyanine, instead of the C_2 symmetry of the macrocycle present in *cis*-PcSn(My_r)₂ (notice that the ligands are highly mobile in the actual systems). Excitation spectra were preferred over absorption spectra for better spectral resolution. The fluorescence excitation spectrum for the tin^{IV} phthalocyanine shows a clear difference in its Q-band shape, which is skewed, in comparison with the Q-band for PcZn, which shows a symmetric and narrower shape (635 cm^{-1} fwhm for *cis*-PcSn(My_r)₂ in comparison with 614 cm^{-1} for PcZn, see also Computational Section). This result is the experimental evidence for a splitting of the first electronic transition that gives rise to the Q-band, which is in turn directly related to a reduction in symmetry of the molecule, in this case, mainly from the double carboxylate anisobidentate coordination in *cis*

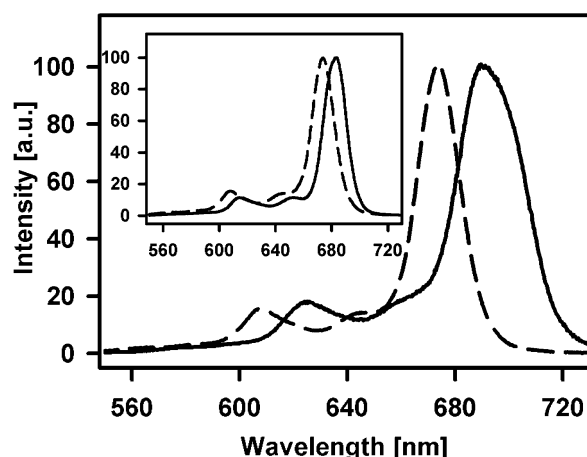


Figure 2. Solid lines: Fluorescence excitation spectra of the phthalocyanines of this study: *cis*-PcSn(Myrr)₂ (main plot) and *trans*-PcSi(Myrr)₂ (inset). The detection wavelength was 720 nm. For comparison, we include the excitation spectrum for zinc phthalocyanine taken in the same solvent (dashed lines both in the inset and in the main graph).

stereochemistry. In fact, such behavior has been reported in some aluminum phthalocyanines where the interaction of water molecules with aluminum phthalocyanine causes a significant decrease in the symmetry of the molecule and, thus, a Q-band splitting.³⁰ Another related case is observed in a magnesium mesoporphyrin where Q-band splitting is attributed to the nonplanar structure of this compound, similar to the case of the *cis*-PcSn(Myrr)₂.³⁰

The emission spectra shown in Figure 1 correspond to emission quantum yields of 0.26 ± 0.03 for the silicon phthalocyanine, and only 0.03 ± 0.01 for the tin macrocycle. Such a low fluorescence yield will be related directly to the observed photophysical channels described below.

Time Resolved Spectroscopy. The fluorescence up-conversion measurements for silicon and tin phthalocyanines are shown in Figure 3. In both cases, there is a rapid onset of the emission in the region of the Q-band, which is produced by the population of the S_1 state after internal conversion from the initially populated upper singlet states S_n with 387.5 nm excitation (main plots of Figure 3, detection wavelength: 720 nm, note that the initial emission onset is unresolved). Once this signal is generated, it decays in a slower time scale with components of up to a few hundred picoseconds for the tin^{IV} phthalocyanine and 3.6 ns for the silicon macrocycle. These signals are discussed in more detail in a later paragraph.

In the insets of Figure 3, we show fluorescence up-conversion results detecting short-lived emissions at energies below that of the B-band: 500 and 540 nm for *cis*-PcSn(Myrr)₂ and *trans*-PcSi(Myrr)₂, respectively. These emission signals only exist during the first 500 fs and, from their spectral position, correspond to photons emitted from the initially formed upper S_n states ($S_n \rightarrow S_0 + h\nu$ emission) during internal conversion to the first excited singlet. The decays of the emission from the upper singlet states are sub-190 fs for *cis*-PcSn(Myrr)₂ and sub-240 fs for *trans*-PcSi(Myrr)₂, and are congruent with the unresolved initial signal rise at 720 nm. These measurements of the internal conversion times within the singlet manifold are valuable experimental observations, since they are reference points in the development of concepts about the dynamics of upper excited states (S_n) in large chromophores.³¹ More

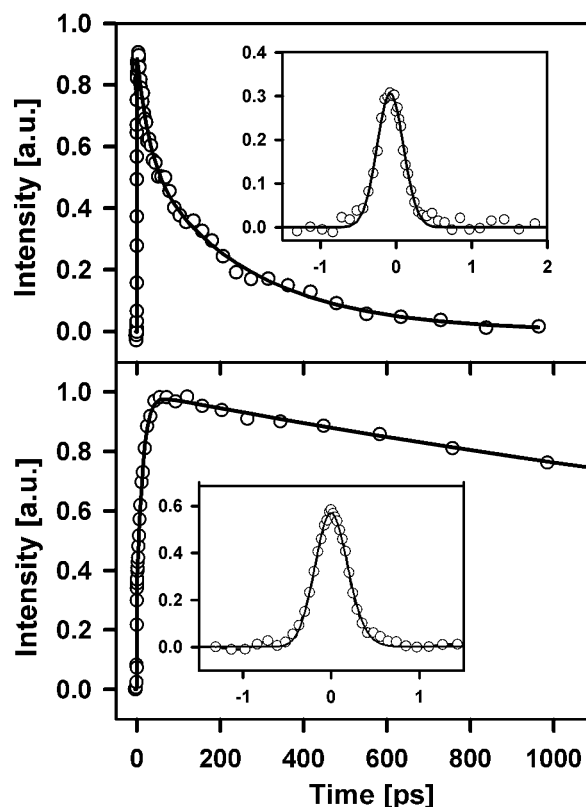


Figure 3. Main plots: Fluorescence up-conversion experiments for *cis*-PcSn(Myrr)₂ (top) and *trans*-PcSi(Myrr)₂ (bottom) in CH₂Cl₂ solution. The detection wavelength was 720 nm, and the excitation wavelength was 387.5 nm. The insets show, respectively, the traces for 500 nm fluorescence detection for *cis*-PcSn(Myrr)₂ (top) and 540 nm detection for *trans*-PcSi(Myrr)₂ (bottom).

specifically, the S_n state decay times of these two systems are significantly shorter than those observed for several tetraphenylporphyrins and porphyrins, which actually do follow the simple $S_2 \rightarrow S_1$ energy gap law (weak to strong coupling cases), with S_2 decay times of up to several picoseconds (S_2 in those cases assigned to the B-band transitions and S_1 to Q-band transitions).^{31,32} As will be discussed below in the Computational Section, the very short ~ 200 fs lifetime of the upper state emissions for the systems of our study are very likely related to the presence of nearly dark, intermediate states between the Q- and B-band transitions. Such states can act as mediators accelerating the nonradiative relaxation after 387.5 nm excitation, producing multistep processes between highly coupled states.³³

Returning to the description of the 720 nm fluorescence emission from the first singlet excited states (Figure 3), after their instrument limited initial onset, they show a double exponential behavior for both phthalocyanines in the picosecond to nanosecond range. It should be noticed that the fluorescence was resolved at this wavelength given that the center of the main vibroelectronic emission peak nearly coincides with the first absorption. For the *trans*-PcSi(Myrr)₂, we observed a rising exponential of about 10 ps, which is followed by a much slower (fluorescence lifetime) decay of 3.6 ns in dichloromethane solution. The first exponential is most likely related to vibrational relaxation within the S_1 state and related to a reshaping of the band as observed at this wavelength. For the tin^{IV} phthalocyanine, both exponentials

are decaying terms, the first one of 30 ps, which is followed by the lifetime decay of 300 ps. The first exponential terms (10 and 30 ps, respectively) are necessarily related to the fact that S_1 is populated nearly instantaneously by internal conversion (~ 200 fs) and, therefore, is formed promptly with excess vibrational energy for both molecules. On the other hand, the 300 ps S_1 population lifetime of *cis*-PcSn(My r) $_2$ is one of the most important observations of this contribution, since it corresponds to a much shorter lifetime and lower fluorescence quantum yield in comparison with other phthalocyanines with a central element with a closed shell electron configuration, including planar tin macrocycles.^{9,10}

In order to explore the pathway for the fast fluorescence decay in *cis*-PcSn(My r) $_2$, we performed the transient absorption experiments of Figures 4 and 5. As can be seen, across the

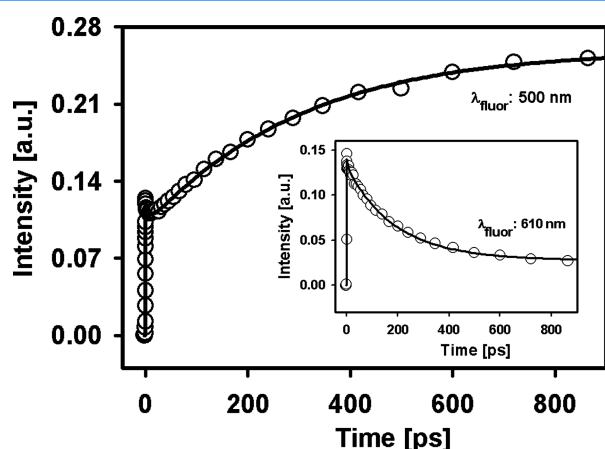


Figure 4. Transient absorption results for *cis*-PcSn(My r) $_2$ in CH_2Cl_2 solution. The excitation wavelength was 387 nm.

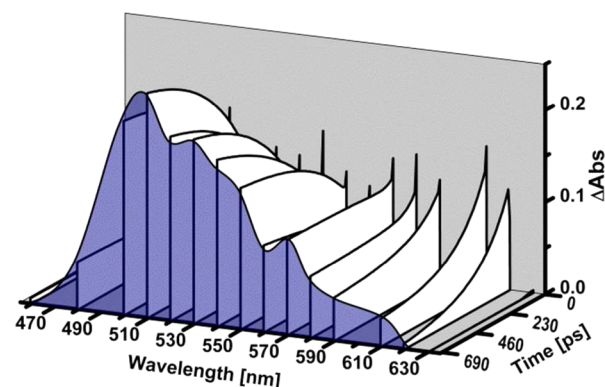


Figure 5. Transient absorption traces and spectrum at 700 ps for *cis*-PcSn(My r) $_2$ in CH_2Cl_2 solution. The excitation wavelength was 387 nm. The line and shadow at 700 ps correspond to a spline interpolation of the single wavelengths for ease of visualization.

spectrum, the traces have small subpicosecond components, which are assigned to relaxation events given that the system is initially formed in an upper singlet as mentioned. On the red side of the transient spectra, above 590 nm, the rapid components are followed by a 300 ps decay to a constant level, while, for wavelengths below 580 nm, the transient absorption signals show increments with time constants of 300 ps (at approximately 570 nm, an isosbestic behavior is seen). Overall, the absorbance signals evolve, forming a long-lived ($\tau \gg 10$ ns) transient spectrum, which is characterized by a

maximum at 510 nm, as can be seen in Figure 5. This spectrum (see 700 ps) matches perfectly with the $T_1 \rightarrow T_n$ absorption spectrum of several other phthalocyanines,^{34–40} and accordingly, we conclude that the fast fluorescence decay is determined by a fast and efficient intersystem crossing (ISC) which populates the triplet manifold of the *cis*-PcSn(My r) $_2$ with a time constant of 300 ps (see also $^1\text{O}_2$ production below as confirmation).

Actinometry and Singlet Oxygen Yield. In order to estimate the yield for triplet formation, we performed a chemical actinometry experiment where equally absorbing solutions of *cis*-PcSn(My r) $_2$ and 1-nitropyrene (387.5 nm) were studied in back-to-back experiments, so that the relative transient absorption signals can be used to measure the ISC yield. These measurements are shown in Figure 6 where the 1-

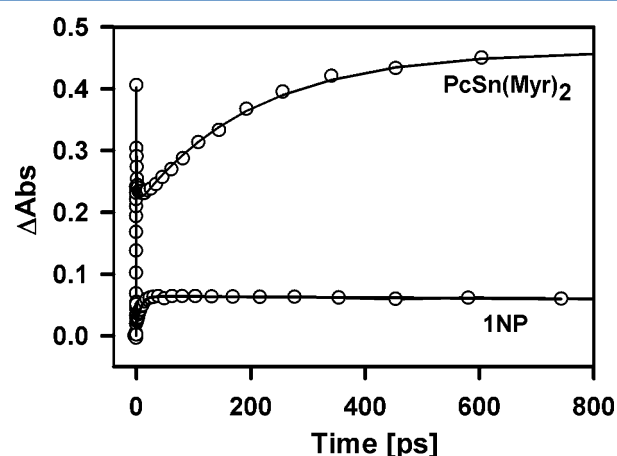


Figure 6. Transient absorption traces for *cis*-PcSn(My r) $_2$ in CH_2Cl_2 solution and 1-nitropyrene (1NP) in acetonitrile solution, taken in back-to-back experiments with identical focusing for excitation and detection. The excitation wavelength was 387.5 nm, and the detection wavelength was 510 nm. The concentrations were adjusted to have the exact same absorbance (0.6) at the excitation wavelength.

nitropyrene solutions show a few picoseconds rise to a constant level. This rise in 1-nitropyrene corresponds to the rapid evolution of 1-nitropyrene from S_1 to T_1 as determined by the groups of Crespo-Hernandez and Vauthey.^{41–43} Since the triplet yield and the 510 nm T_1 absorption coefficient of 1-nitropyrene are known,⁴⁴ the *cis*-PcSn(My r) $_2$ signals at 510 nm give a measure for the triplet production yield as follows: Taking all the published values for the $T_1 \rightarrow T_n$ absorption coefficient, which have been determined for several phthalocyanines,^{34–40} we conclude that the triplet yield for *cis*-PcSn(My r) $_2$ ranges from 0.89 to 0.97 (corresponding to $\epsilon_{T_1} = 37 \times 10^3 \text{ M}^{-1} \text{ cm}^{-1}$ and $\epsilon_{T_1} = 34 \times 10^3 \text{ M}^{-1} \text{ cm}^{-1}$, respectively, at 510 nm). The upper limit takes into account the 0.03 fluorescence quantum yield, and the lower limit considers the largest $T_1 \rightarrow T_n$ triplet absorption coefficient ever reported for a phthalocyanine.³⁹ As can be seen, the 300 ps ISC makes this tin^{IV} macrocycle have a very efficient triplet yield formation which can be valuable for applications which require, for example, electron transfer or molecular oxygen sensitization through triplet states.⁴⁵

The singlet oxygen production efficiency was measured through a scheme that used the ESR signals from the TEMPO adduct, which can accurately measure the production singlet oxygen. The $^1\text{O}_2$ quantum yield $\phi(^1\text{O}_2)$ was determined from

the generation rate of singlet oxygen $R(^1\text{O}_2)$ and the flux of absorbed photons, I_a , (the methodology to determine I_a is described in the Supporting Information): $\phi(^1\text{O}_2) = R(^1\text{O}_2)/I_a$.¹⁶

TEMP reacts with $^1\text{O}_2$ to give the adduct TEMPO, a stable nitroxide free radical with an appropriate detection limit, compared with other spin traps (see the Supporting Information). This method is sensible and selective in the detection of $^1\text{O}_2$, and no interference from other possible side products could affect the reaction between TEMP and $^1\text{O}_2$.⁴⁶ Upon irradiating solutions of TEMP and phthalocyanine in air-saturated ethanol, a time-accumulating ESR spectrum is obtained. This spectrum is characteristic of TEMPO ($g = 2.006$ and $a_N = 16.2$ G) consisting of three equally intense lines (see inset in Figure 7).^{16,46} In the absence of light or

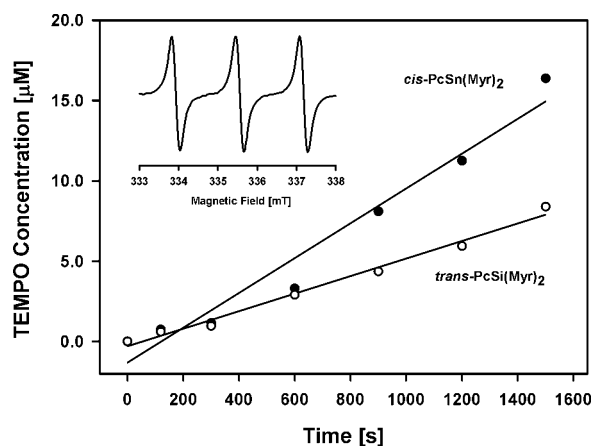


Figure 7. ESR results for air-equilibrated ethanol solutions of *cis*-PcSn(Myristate)₂ (solid symbols) and *trans*-PcSi(Myristate)₂ (empty symbols). The inset shows the ESR spectrum of the observed TEMPO adduct.

phthalocyanine (not shown), no ESR signal was detected. When the sample was degassed by bubbling with N₂ for 10 min, the intensity of the ESR signal decreased to the baseline level, showing that oxygen is also indispensable for generating the signal.

Figure 7 shows the formation of TEMPO as a function of irradiation time by using *cis*-PcSn(Myristate)₂ and *trans*-PcSi(Myristate)₂ in aerated ethanol solutions (showing zero order kinetics for TEMPO production, which implies steady state kinetics for $^1\text{O}_2$).⁴⁵ The formation rate of TEMPO, and therefore the formation rate of $^1\text{O}_2$, was calculated from the slope of this plot. Thus, $R(^1\text{O}_2)$ was found to be 1.1×10^{-8} M s⁻¹ for *cis*-PcSn(Myristate)₂ and 0.5×10^{-9} M s⁻¹ for *trans*-PcSi(Myristate)₂. According to these results, the quantum yield of $^1\text{O}_2$ (ϕ_Δ) was found to be 0.22 ± 0.05 for *cis*-PcSn(Myristate)₂ and 0.1 ± 0.05 for *trans*-PcSi(Myristate)₂ in the air equilibrated ethanol solutions. Thus, the tin macrocycle was approximately twice as fast for the production of $^1\text{O}_2$ species in ethanol in comparison to its silicon analogue.

Computational Results. The main objective of our computational work was to make an initial description of the electronic structure of the half-domed or cap-shaped tin^{IV} macrocycle and relate it to the overall observed spectra, ultrafast $S_n \rightarrow S_1$ internal conversion (insets in Figure 3), and loss of degeneracy in the first transition. The geometry optimization at the PBE/3-21G level of theory produces *trans*-PcSi(Myristate)₂ and *cis*-PcSn(Myristate)₂ structures that are very

congruent with the previously reported X-ray diffraction data for both compounds (see images and tables in the Supporting Information). The root mean square deviations (RMSDs) with respect to the crystalline geometries are only 0.106 and 0.114 Å for the tin^{IV} and silicon^{IV} compounds, respectively (takes into account only the non-hydrogen atoms, not including those of the myristate chains which are likely to fluctuate significantly when the molecule is not in the crystalline form and subject to molecular packing and crowding).

The TD-DFT results at the PBE/6-311++G** + LB94 + CRENBL ECP (Sn) level indicate that there are two non-degenerate electronic transitions in the Q-band region for both phthalocyanines. As mentioned previously, this confirms the description in terms of the anisotropic axial bonding through carboxylate groups, which makes the systems lose the D_{4h} macrocyclic symmetry and behave as mentioned in the steady state results section. Also, the results from the TD-DFT theoretical calculations indicate that the states associated with the Q-bands of the macrocycles are dominated by transitions between the HOMO and LUMO and LUMO+1 (Kohn–Sham orbitals), as summarized in the Supporting Information. With this result, it is clear that the general Gouterman type description for this band is maintained even for the non-planar system. The gas phase calculations at this level of theory actually overestimate the band center in the tin^{IV} macrocycle by only 230 cm⁻¹ (considering the average of the calculated transitions), and slightly underestimate the Q-band center for the Si macrocycle by just 120 cm⁻¹.

Qualitatively consistent with the observed spectra, the TD-DFT calculations show a group of more than 15 bands in a spectral region similar to that of the B-band. This can be compared with previous TD-DFT calculations for the highly symmetric ZnPc which show between five and six transitions in this spectral zone, depending on the type of functional used (pure versus hybrid).²³ Clearly, the presence of several nondegenerate transitions in the 350–450 nm region for the present systems again is related to the symmetry reduction. The calculated transitions assigned to the B-band in our calculations appear systematically at lower energies when compared with the experimental B-band maxima (362 nm for the Si case and 358 nm for the Sn case).

Importantly, the TD-DFT calculations predict the existence of $n-\pi^*$, nearly dark states between the Q-band states and the B-band states (480–600 nm, 7 states for the Si case and 10 for the Sn macrocycle). The spectral position of these states is depicted with their oscillator strengths in the insets of Figures 8 and 9. Although it has been shown that the exact energy of these transitions depends on the calculation (type of functional and base quality), the presence of this kind of states has been verified in previous calculations for other phthalocyanines,²³ which show that they are predicted to appear, like in our cases, near the low energy end of the B transitions and the high energy end of the Q transitions. Such states are very likely to influence the dynamics of the upper singlet states (formed by excitations to the B-band as in our experiments). For our systems, we postulate that these states may act as intermediary states in the ultrafast cascade-type internal conversion that populates the fluorescent S_1 states in ~200 fs both *trans*-PcSi(Myristate)₂ and *cis*-PcSn(Myristate)₂.³³ In any case, the description of the decay dynamics upon excitation into B-band states needs to take into account the presence of these states which might be relevant in applications like electron or energy transfer, and in some cases ligand dissociation reactions.

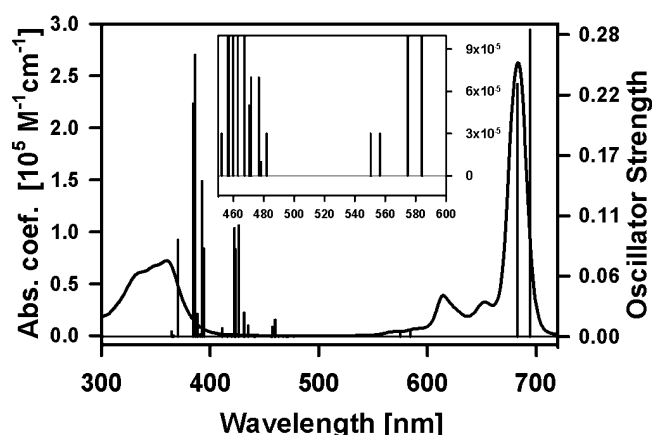


Figure 8. Absorption spectrum and calculated electronic transitions at the TD-DFT level for *trans*-PcSi(Myrr)₂. The inset shows the spectral positions of nearly forbidden transitions in the region between the B-band and the Q-band.

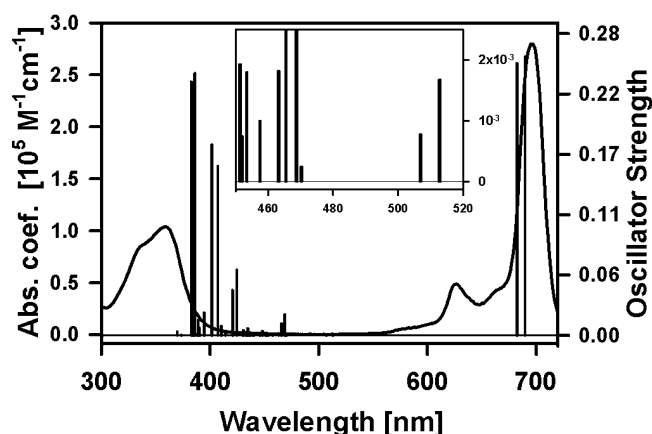


Figure 9. Absorption spectrum and calculated electronic transitions at the TD-DFT level for *cis*-PcSn(Myrr)₂. The inset shows the spectral position of nearly forbidden transitions in the region between the B-band and the Q-band.

CONCLUSIONS

We have characterized the photophysical properties of a *cis* disubstituted phthalocyanine. The time scale for the internal conversion process gives rise to the S_1 fluorescent state in a time scale of approximately 200 fs upon excitation in the Soret band (387.5 nm). Once this state is formed and relaxed, it decays with a time constant of 300 ps populating the triplet manifold with more than 80% efficiency for *cis*-PcSn(Myrr)₂. In comparison, a silicon phthalocyanine with the same substituents but bonded in a *trans* configuration has a much longer fluorescent lifetime in the nanosecond regime. The rapid intersystem crossing in *cis*-PcSn(Myrr)₂ is attributed in part to the large nuclear charge of the Sn central atom, but from comparisons with other tin macrocycles, it appears that its nanocapped (half-domed) conformation may contribute to the efficient coupling of S_1 with the first triplet state, probably due to the contribution of p_x and p_y atomic orbitals to the orbitals involved in the excitation to the first singlet state. Thus, the nonplanarity could increment spin orbit coupling to the triplet manifold. Calculations at the TD-DFT level of theory give a good description of the observed electronic transitions, showing that the common Q-band structure is maintained in the nanocapped macrocycle. In addition and in accordance with

previous calculations, the TD-DFT method predicts the presence of $n-\pi^*$ at transition energies between the B- and Q-bands. Such states are likely to participate in the ultrafast internal conversion that populates the S_1 state in the ultrafast primary photoinduced step.

The photophysical properties and improved solubility make *cis*-PcSn(Myrr)₂ an interesting system from the applications point of view; therefore, its capacity to induce the formation of singlet oxygen was evaluated by measuring the formation of TEMPO adducts through an ESR method. The 1O_2 yield in alcohols was determined to be significantly larger than that observed for the planar phthalocyanine.

ASSOCIATED CONTENT

Supporting Information

Details of the ESR measurements for the singlet oxygen determinations, optimized geometries, and comparisons with the X-ray determined geometries. Description of the calculated transitions associated with the Q-band. This material is available free of charge via the Internet at <http://pubs.acs.org>.

AUTHOR INFORMATION

Corresponding Author

*E-mail: jpeon@servidor.unam.mx.

Notes

The authors declare no competing financial interest.

ACKNOWLEDGMENTS

For financial support, we thank CONACyT Grant 178541 and PAPIIT-UNAM Grant IN 204211. G.G. thanks DGAPA-UNAM for a postdoctoral grant. J.P. acknowledges support from PROMEP-UAEM, CA-86, CA-110. J.Z.R. acknowledges access to computational resources from Laboratorio de Supercómputo y Visualización en Paralelo, U.A.M. Iztaapalapa.

REFERENCES

- (1) Gurol, I.; Durmus, M.; Ahsena, V.; Nyokong, T. *Dalton Trans.* **2007**, 3782–3791.
- (2) Idowu, M.; Nyokong, T. *J. Photochem. Photobiol., A* **2008**, *199*, 282–290.
- (3) Rodriguez-Cordoba, W.; Noria, R.; Guarin, C. A.; Peon, J. *J. Am. Chem. Soc.* **2011**, *133*, 4698–4701.
- (4) Beltran, H. I.; Esquivel, R.; Lozada-Cassou, M.; Dominguez-Aguilar, M. A.; Sosa-Sanchez, A.; Sosa-Sanchez, J. L.; Hopfl, H.; Barba, V.; Luna-Garcia, R.; Farfan, N.; et al. *Chem.—Eur. J.* **2005**, *11*, 2705–2715.
- (5) Beltran, H. I.; Esquivel, R.; Sosa-Sanchez, A.; Sosa-Sanchez, J. L.; Hopfl, H.; Barba, V.; Farfan, N.; Garcia, M. G.; Olivares-Xometl, O.; Zamudio-Rivera, L. S. *Inorg. Chem.* **2004**, *43*, 3555–3557.
- (6) Sosa-Sanchez, J. L.; Galindo, A.; Gnecco, D.; Bernes, S.; Fern, G. R.; Silver, J.; Sosa-Sanchez, A.; Enriquez, R. G. *J. Porphyrins Phthalocyanines* **2002**, *6*, 198–202.
- (7) Sosa-Sanchez, J. L.; Sosa-Sanchez, A.; Farfan, N.; Zamudio-Rivera, L. S.; Lopez-Mendoza, G.; Flores, J. P.; Beltran, H. I. *Chem.—Eur. J.* **2005**, *11*, 4263–4273.
- (8) Bennett, W. E.; Broberg, D. E.; Baenzige, Nc. *Inorg. Chem.* **1973**, *12*, 930–936.
- (9) Masilela, N.; Nyokong, T. *Dyes Pigm.* **2011**, *91*, 164–169.
- (10) Pelliccioli, A. P.; Henbest, K.; Kwag, G.; Carvagno, T. R.; Kenney, M. E.; Rodgers, M. A. J. *J. Phys. Chem. A* **2001**, *105*, 1757–1766.
- (11) Zugazagoitia, J. S.; Maya, M.; Damian-Zea, C.; Navarro, P.; Beltran, H. I.; Peon, J. *J. Phys. Chem. A* **2010**, *114*, 704–714.
- (12) Plaza-Medina, E. F.; Rodriguez-Cordoba, W.; Morales-Cueto, R.; Peon, J. *J. Phys. Chem. A* **2011**, *115*, 577–585.

- (13) Zugazagoitia, J. S.; Collado-Fregoso, E.; Plaza-Medina, E. F.; Peon, J. *J. Phys. Chem. A* **2009**, *113*, 805–810.
- (14) Hess, G. C.; Kohler, B.; Likhovotvorik, I.; Peon, J.; Platz, M. S. *J. Am. Chem. Soc.* **2000**, *122*, 8087–8088.
- (15) Collado-Fregoso, E.; Zugazagoitia, J. S.; Plaza-Medina, E. F.; Peon, J. *J. Phys. Chem. A* **2009**, *113*, 13498–13508.
- (16) Sun, L. Z.; Bolton, J. R. *J. Phys. Chem.* **1996**, *100*, 4127–4134.
- (17) Perdew, J. P.; Burke, K.; Ernzerhof, M. *Phys. Rev. Lett.* **1996**, *77*, 3865–3868.
- (18) Perdew, J. P.; Burke, K.; Ernzerhof, M. *Phys. Rev. Lett.* **1997**, *78*, 1396–1396.
- (19) Binkley, J. S.; Pople, J. A.; Hehre, W. J. *J. Am. Chem. Soc.* **1980**, *102*, 939–947.
- (20) Dobbs, K. D.; Hehre, W. J. *J. Comput. Chem.* **1986**, *7*, 359–378.
- (21) Dobbs, K. D.; Hehre, W. J. *J. Comput. Chem.* **1987**, *8*, 880–893.
- (22) Gordon, M. S.; Binkley, J. S.; Pople, J. A.; Pietro, W. J.; Hehre, W. J. *J. Am. Chem. Soc.* **1982**, *104*, 2797–2803.
- (23) Nemykin, V. N.; Hadt, R. G.; Belosludov, R. V.; Mizuseki, H.; Kawazoe, Y. *J. Phys. Chem. A* **2007**, *111*, 12901–12913.
- (24) Clark, T.; Chandrasekhar, J.; Spitznagel, G. W.; Schleyer, P. V. *J. Comput. Chem.* **1983**, *4*, 294–301.
- (25) Krishnan, R.; Binkley, J. S.; Seeger, R.; Pople, J. A. *J. Chem. Phys.* **1980**, *72*, 650–654.
- (26) Hurley, M. M.; Pacios, L. F.; Christiansen, P. A.; Ross, R. B.; Ermler, W. C. *J. Chem. Phys.* **1986**, *84*, 6840–6853.
- (27) Ross, R. B.; Powers, J. M.; Atashroo, T.; Ermler, W. C.; Lajohn, L. A.; Christiansen, P. A. *J. Chem. Phys.* **1990**, *93*, 6654–6670.
- (28) Bylaska, W. A. d. J.; Govind, N.; Kowalski, K.; Straatsma, T. P.; Valiev, M.; Wang, D.; Apra, E.; Windus, T. L.; Hammond, J.; Nichols, P.; et al. *NWChem*; Pacific Northwest National Laboratory, Richland, WA, 2009; pp A Computational Chemistry Package for Parallel Computers, version 5.1.1.
- (29) Kendall, R. A.; Apra, E.; Bernholdt, D. E.; Bylaska, E. J.; Dupuis, M.; Fann, G. I.; Harrison, R. J.; Ju, J. L.; Nichols, J. A.; Nieplocha, J.; et al. *Comput. Phys. Commun.* **2000**, *128*, 260–283.
- (30) Reinot, T.; Hayes, J. M.; Small, G. J.; Zerner, M. C. *Chem. Phys. Lett.* **1999**, *299*, 410–416.
- (31) Liu, X.; Tripathy, U.; Bhosale, S. V.; Langford, S. J.; Steer, R. P. *J. Phys. Chem. A* **2008**, *112*, 8986–8998.
- (32) Tripathy, U.; Kowalska, D.; Liu, X.; Velate, S.; Steer, R. P. *J. Phys. Chem. A* **2008**, *112*, 5824–5833.
- (33) Migani, A.; Leyva, V.; Feixas, F.; Schmierer, T.; Gilch, P.; Corral, I.; Gonzalez, L.; Blancafort, L. *Chem. Commun.* **2011**, *47*, 6383–6385.
- (34) Byeon, C. C.; McKerns, M. M.; Sun, W. F.; Nordlund, T. M.; Lawson, C. M.; Gray, G. M. *Appl. Phys. Lett.* **2004**, *84*, 5174–5176.
- (35) DeRosa, M. C.; Crutchley, R. J. *Coord. Chem. Rev.* **2002**, *233*, 351–371.
- (36) Gunaratne, T.; Kennedy, V. O.; Kenney, M. E.; Rodgers, M. A. J. *J. Phys. Chem. A* **2004**, *108*, 2576–2582.
- (37) Jacques, P.; Braun, A. M. *Helv. Chim. Acta* **1981**, *64*, 1800–1806.
- (38) Pelliccioli, A. P.; Henbest, K.; Kwag, G.; Carvagno, T. R.; Kenney, M. E.; Rodgers, M. A. J. *J. Phys. Chem. A* **2001**, *105*, 1757–1766.
- (39) Pyatosin, V. E.; Tsvirko, M. P. *Zh. Prikl. Spektrosk.* **1980**, *33*, 320–325.
- (40) Wang, S. Q.; Gan, Q.; Zhang, Y. F.; Li, S. Y.; Xu, H. J.; Yang, G. Q. *ChemPhysChem* **2006**, *7*, 935–941.
- (41) Crespo-Hernandez, C. E.; Burdzinski, G.; Arce, R. *J. Phys. Chem. A* **2008**, *112*, 6313–6319.
- (42) Mohammed, O. F.; Vauthey, E. *J. Phys. Chem. A* **2008**, *112*, 3823–3830.
- (43) Plaza-Medina, E. F.; Rodriguez-Cordoba, W.; Peon, J. *J. Phys. Chem. A* **2011**, *115*, 9782–9789.
- (44) Arce, R.; Pino, E. F.; Valle, C.; Negron-Encarnacion, I.; Morel, M. J. *J. Phys. Chem. A* **2011**, *115*, 152–160.
- (45) Nyokong, T. *Coord. Chem. Rev.* **2007**, *251*, 1707–1722.
- (46) Rinalducci, S.; Pedersen, J. Z.; Zolla, L. *Biochim. Biophys. Acta, Bioenerg.* **2004**, *1608*, 63–73.